Silicon Reconfigurable Electro-Optical Logic Circuit Enabled by a Single-Wavelength Light Input

Yu Qi, Ciyuan Qiu, *Member, IEEE*, Weilu Gao, Xin Zhong, and Yikai Su, *Senior Member, IEEE*

***Abstract*— Here, we demonstrate a silicon reconfigurable electro-optical directed-logic circuit enabled by a single-wavelength light input based on optical switches and photodetectors (PDs). Each switch consists of a silicon micro-ring resonator with an embedded p-n junction for logic input and a micro-heater for reconfiguration. The PDs have integrated p-i-n junctions for photocurrents generation which can eliminate the optical interference in the signal-wavelength calculation. This scalable circuit can be reconfigured to perform any combinational logic operation with a single wavelength light input. For a proof of concept demonstration, arbitrary two-input combinational logic functions with speeds up to ∼270 Mb/s were implemented successfully.**

***Index Terms*— Reconfigurable, electro-optical logic, single-wavelength.**

I. Introduction

RECONFIGURABLE and cellular optical directed-logic circuits provide an optics-inspired paradigm to perform different Boolean functions with a low latency [1], [2]. In an electro-optical (EO) directed-logic circuit, each switch is controlled by an operand and the operation of each switch is independent on the operations of the other switches. All switches perform their operations simultaneously, thus switching times do not accumulate with circuit elements [3]–[5]. This simultaneous switching stands different from traditional electronic logic architectures, wherein each gate must wait for the result of previous gates and thus gate delays are cascaded, resulting in increased latencies with increased gates. Thanks to the fast and low-loss propagation of light, the whole latency for the optical directed-logic circuit can thus be very low which depends on the group delay of light in the photonic circuit. Furthermore, the reconfiguration paradigm can be used to calculate different complicated logic functions with fast reconfigurability. The low latency and fast reconfigurability of reconfigurable directed-logic circuits make them useful for optical computing, package routing as well as real-time applications such as video analysis and recognition-and-analysis of fast-moving objects, where low latency and function reconfiguration are desired [2], [4].

Several silicon reconfigurable electro-optical logic circuits enabled by multi-spectral light inputs have been demonstrated [3], [4], according to the sum of products expression for the logic functions. In these proof-of-concept demonstrations, the circuits firstly perform AND operation to obtain the optical logic products, then incoherently add these products (OR operation) in the optical domain. Since it is hard to precisely control the phases of light signals for the optical logic products, one needs to use an individual wavelength for each optical product in order to eliminate the optical interference in the OR operation. Then the number of required light wavelengths is equal to the number of the product terms. Noted that, the general sum-of-product form for an arbitrary logic function Y can be expressed as $Y = P_1 + P_2 + P_3 + \ldots P_n$, where P_i is a product of logic inputs, such as $P_i = a_1\overline{a_2}\cdots a_m$ ($\overline{a_2}$ represents the inverse of a_2, m is the number of the logic inputs). Then, if the number of logic inputs (m) increases for complex logic function calculations, the number of product terms exponentially increases to be on the order of 2^m, so does the number of required wavelengths. In this way, however, the complexity of the multi-spectral input optical system dramatically increases.

Xu and Soref [2, sec. 6.2.1] have proposed an alternative way to perform the logic operations based on the sum of products expression. In that circuit, EO switches in horizontal waveguides perform the AND operations to obtain the optical products and then these products are added by using a parallel-connected PD array in the electronic domain. In this way, the optical interference can be eliminated and the number of required wavelengths could be reduced. However, to date, the proposed concept has not been experimentally verified.

In this Letter, we report a proof-of-concept demonstration for the scalable EO logic circuits as discussed in that section [2]. We further show that the circuit can be enabled by a single-wavelength light input through equally splitting the single-wavelength light input power into the horizontal waveguides. With a 2×2 array of reconfigurable EO switches and a PD array, this logic circuit can perform arbitrary two-input logic functions.

Manuscript received November 9, 2018; revised January 19, 2019; accepted January 29, 2019. Date of publication February 4, 2019; date of current version March 12, 2019. This work was supported in part by the National Natural Science Foundation of China under Grants 61875120 and 61505104, and in part by the Open Fund of IPOC (BUPT). *(Corresponding author: Ciyuan Qiu.)*

Y. Qi, C. Qiu, and Y. Su are with the State Key Laboratory of Advanced Optical Communication Systems and Networks, Department of Electronic Engineering, Shanghai Jiao Tong University, Shanghai 200240, China (e-mail: qiyu1996@sjtu.edu.cn; qiuciyuan@sjtu.edu.cn; yikaisu@sjtu.edu.cn).

W. Gao is with the Department of Electrical and Computer Engineering, Rice University, Houston, TX 77005 USA (e-mail: weilu.gao@rice.edu).

X. Zhong is with the Science and Technology on Electronic Information Control Laboratory, Chengdu 610036, China (e-mail:15497546@qq.com).

Color versions of one or more of the figures in this letter are available online at http://ieeexplore.ieee.org.

Digital Object Identifier 10.1109/LPT.2019.2897130

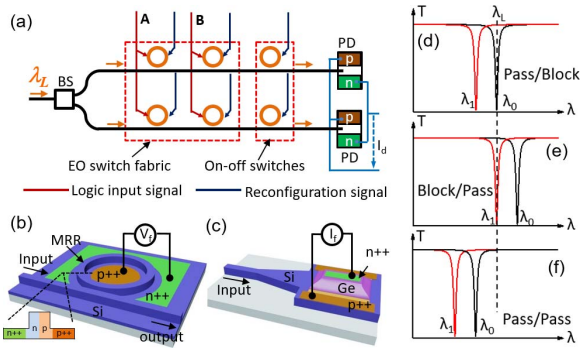

Fig. 1. (a) Layout and the electrical actuation of the logic circuit. BS: Beam splitter. (b) Diagram for a MRR-based EO switch with an embedded p-n junction. (c) Diagram for a Ge-on-Silicon PD. The transmission spectra for a EO switch in three operation modes: (d) *pass/block* mode, (e) *block/pass* mode, (f) *pass/pass* mode [2].

Silicon MRR-based EO switches and Ge-on-silicon PDs are the basic building blocks for this scalable logic circuit. Each EO switch has an embedded p-n junction for logic input and a TiN micro-heater for reconfiguration [3]. The PD has an embedded p-i-n junction for photocurrent generation. The switch and the PD used in the photonic circuit have small size, short switching time, low power consumption, and they are compatible with large-scale integration [6], [7].

II. Device Schematic and Principle

The architecture of our EO logic circuit is schematically shown in Fig. 1(a). It consists of one beam splitter (BS), two-plus-two EO switches, two on-off switches, two Ge-on-silicon PDs and two horizontal waveguides that are marked as black lines. The red lines represent the electronic logic input signals (operands A and B), which are applied on the optical switches. Here each operand simultaneously controls two optical switches in different horizontal waveguides. Monochromatic continuous light with a wavelength λ_L is coupled into the circuit through its input port and then equally spitted into two horizontal waveguide based on the BS. In each horizontal waveguide, light is modulated by two cascaded EO switches and one on-off switch before entering the PD for photocurrent generation.

Each EO switch in the circuit can work in three operation modes, as shown in Figs. 1(d)-1(f). The electronic input logic signal (operands A or B) is applied on the p-n junction of the EO switch as shown in Fig. 1(b) and tune its resonance wavelengths through the free carrier plasma effect of silicon. We denote the resonance wavelength as λ_0 when the logic is '0' and λ_1 when the logic is '1'. The position of λ_0 and λ_1 with respect to the input continuous light wavelength λ_L can be controlled by the reconfiguration signal through the micro-heater by using the thermo-optic effect of silicon. When λ_0 aligns with λ_L as shown in Fig. 1(d), the EO switch works in the *pass/block* mode. In this mode, the transmission is low if the logic input is '0' and is high if the logic input is '1'. Thus the optical logic output will match the electronic logic input. When λ_1 aligns with λ_L as shown in Fig. 1(e), the transmission is low if the logic input is '1' and is high if the logic input is '0'. The switch works in the *block/pass* mode and the optical logic output will be the inverse of the electronic logic input. If neither λ_0 nor λ_1 aligns with λ_L as shown in the Fig. 1(f), the EO switch works in the *pass/pass* mode and the optical logic output is always '1' regardless of the electronic logic input.

Logic products are calculated by reconfiguring the operation modes of the EO switches in the horizontal waveguides. As shown in Fig. 1(a), light can pass the two EO switches connected by a horizontal waveguide (corresponding to an output logic "1") only when the two switches are in the *pass* state. Then a product function (logic AND operation) is obtained in the waveguide on the right side of the two EO switches, depending on their operation modes. For example, if the switch controlled by A is in the *pass/block* mode and the switch controlled by B is in the *block/pass* mode, the optical output carries the product $A\overline{B}$. If the switch controlled by A is in the *pass/pass* mode and the other switch controlled by B is in the *pass/block* mode, the optical output is B. In this way, any two-input product can be obtained by reconfiguring the operation modes of the EO switches.

The light signal that carries the calculated optical logic product is then sent to the PD (as shown in Fig. 1(c)) at the end of the waveguide for photocurrent generation after passing through the MRR based on-off switch. If the product calculated by this waveguide is part of the logic function to be calculated, the on-off switch is in the *pass* state and light will be sent to the PD for photodetection. This can be achieved by tuning the resonance of the MRR of the on-off switch to be off resonance. Otherwise, light will be blocked by the on-off switch and will not be collected by the PD through tuning the resonance of the MRR of the on-off switch to be on resonance. Noted that, the parameters for the on-off switches are the same as the EO switches except that the on-off switches don't have embedded p-n junctions for logic input, they have only micro-heaters.

Then the incoherent sum (OR function) is implemented by adding up all the individual photocurrents which are generated by the parallel-connected Ge-on-silicon PD array. After adding up all the individual generated photocurrents, the PD array creates a combined photocurrent which is then fed to a high-speed oscilloscope. Logic "1" is defined as the combined photocurrent collected if any one of the horizontal waveguides has a high-level output. In this way, the logic functions, expressed as a sum of products, can be calculated.

III. Fabrication and Characterization

The EO logic circuits are fabricated in a CMOS photonics foundry at the Institute of Microelectronics of Singapore. The fabrication starts on a silicon-on-insulator (SOI) wafer with 220-nm-thick top silicon and 2-μm-thick buried oxide. Rib waveguides are used to construct the photonic circuits, which have a width of 500 nm, a height of 220 nm, and a slab thickness of 90 nm, respectively. This waveguide geometry supports single-mode propagation for TE-polarized waves at a wavelength of 1550 nm. Each switch consists of a MRR with a diameter of 30 μm, which is side-coupled to the straight waveguide. The gap width is set to 350 nm. At the end of

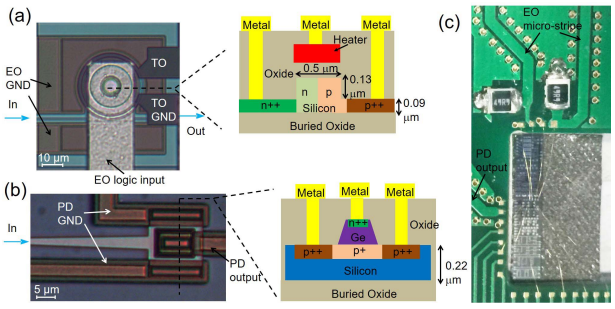

Fig. 2. (a) Optical micrograph of the EO switch. (b) Optical micrograph of the Ge-on-silicon PD. The insert figures in (a) and (b) are the cross-sectional diagrams for the switch and the PD, respectively. (c) Device mounted on a stage and wire-bonded to a PCB board.

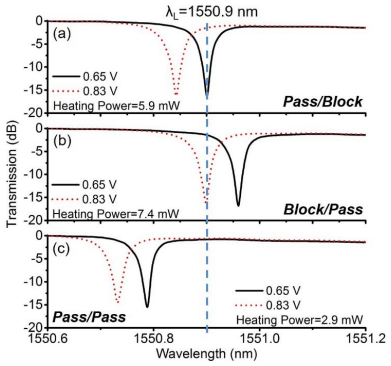

Fig. 3. Measured transmission spectra for an EO switch in three operation modes: (a) *pass/block* mode, (b) *block/pass* mode, (c) *pass/pass* mode. The applied modulation signal is 0.65 V and 0.83 V, respectively. In this experiment, p-n junctions work in carrier-injection mode.

the rib waveguide, the evanescent-wave coupled Ge-on-silicon photodetector is integrated. A deep-UV lithography process is used to define the device pattern, which is etched into the silicon layer by inductively coupled plasma etching. Following the etching, the p++, p, n++, and n implants for the silicon switches and the p-type doping for anode formation of the Ge-on-silicon photodetectors are performed on the exposed silicon as shown in the inset figures of Fig. 2(a) and Fig. 2(b), respectively. Then epitaxial 500-nm-thick germanium is selectively grown on top of the silicon. To form the contact of a photodetector, an n++ doping region is defined on the top of Ge layer with phosphorus implant. A 2.25-μm-thick SiO_2 layer is then deposited onto the wafer using plasma enhanced chemical vapor deposition (PECVD). A 120-nm-thick titanium nitride (TiN) layer is sputtered and then patterned on the oxide to form the micro-heaters. Another 500-nm-thick SiO_2 layer is then deposited by PECVD. Finally, vias are opened, and a 2-μm-thick aluminum layer is sputtered and etched to form the electric connections for the p-n junctions and the micro-heaters. After device fabrication, the contact pads on the chip are wire-bonded to a custom-made interface board, as shown in Fig. 2(c). Each micro-heater is controlled by a power source. The p-n junctions of the switches and the PDs are wire-bonded to SMA connectors. For the electronic logic input signals applied to the switches, 50-Ω terminal resistors are integrated to satisfy the impedance matching condition.

The transmission spectra of the TE mode of an EO switch were measured with a tunable laser. When the bias voltage applied on the p-n junction is 0.65 V, the transmission spectrum has a sharp resonance dip, as shown in Fig. 3(a). The loaded quality factor is about 35,200. When the forward bias voltage increases from 0.65 V to 0.83 V, more free carriers are injected into the p-n junction. Therefore, the loss of the cavity will increase and the refractive index will decrease. Accordingly, the resonance blue shifts and the quality factor decreases slightly to 28,700, as shown in Fig. 3(a). At the input laser wavelength of $\lambda_L = 1550.9$ nm, the optical transmission is high when the bias voltage is high at 0.83 V (logic "1") and the transmission is low when the bias voltage is low at 0.65 V (logic "0"). Thus the EO switch works in the *pass/block* mode. We can also control the operation mode of the EO switch to be *block/pass* mode or *pass/pass* mode by changing the applied heating power on the micro-heater, as shown in Fig. 3(b) and Fig. 3(c), respectively. In all transmission spectra, the depth of the resonance dip exceeds 10 dB, promising high extinction ratios for optical switching.

The optical properties for the Ge-on-silicon PDs were also characterized. To enhance the responsivity, the single-mode waveguide is firstly tapered to multi-mode waveguide, and then the PD is integrated at the end, as shown in Fig. 2(b). The width and length for the PDs are 19 μm and 14 μm, respectively. The responsivity for the PD is measured to be about 0.31 A/W at 0 V bias. This type of detector should be able to work at a speed of multi-GHz [7].

IV. Reconfigurable Logic Operation and Discussion

All the sixteen possible two-input logic functions were demonstrated in the experiment by reconfiguring the operation modes of the switches. Due to limitations of space, we show only eight of all the sixteen logic functions as representatives. The working wavelength is set to 1550.9 nm for all demonstrations. The two logic input signals are fixed with a bit rate of 270 Mb/s with voltage ranges from 0.65 V (logic "0") to 0.83 V (logic "1"). Thus, the maximum peak-to-peak voltage (V_{pp}) for each logic input is 0.18 V. Here the logic input signals with low V_{pp} are chosen to decrease their radio frequency (RF) radiation, which will create noise on the electronic logic output signal from the PD array since the bonding wires can be considered as RF antennas [8]. The total consumed RF power is about 120 μW, and the total heating power used in the demonstration ranges from 64 mW to 66 mW for the different logic functions. The thermal-optic reconfiguration time is measured to <40 μs. The output power of the laser is 2 dBm. A grating coupler is used to couple light into the input waveguide whose coupling loss is about ~6.3 dB. Noted that, the coupling loss is extracted by measuring another pair of identical grating couplers connected by a straight waveguide on the same chip.

The circuit diagrams for different logic functions are shown in Figs. 4(a)-4(h) by reconfiguring the operational modes of the EO switches and on-off switches. The corresponding electronic output signals are shown in Figs. 5(a)-5(h). In Figs. 5(a) and 5(b), the logic output signals are the same as the logic input signals A and B, respectively. In Figs. 5(a)-5(d), the logic function has only one product thus only light

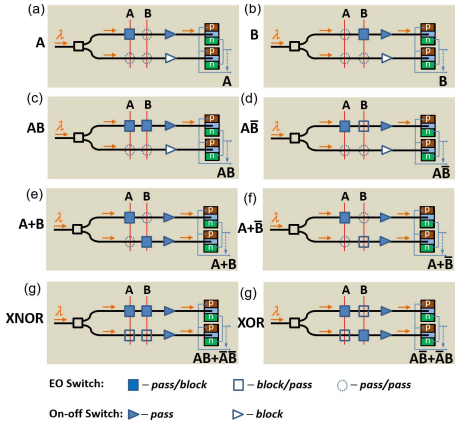

Fig. 4. Logic circuit diagrams for different two-input logic functions.

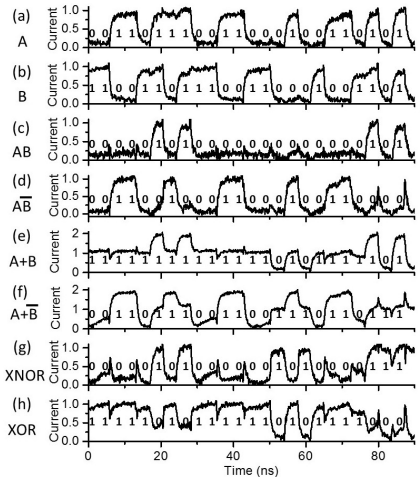

Fig. 5. Waveforms of the output electronic current signal from the two input logic circuits shown in Fig. 4. The two logic input signals are non-return-to-zero (NRZ) 2^7-1 pseudorandom bit sequence signals at 270 MHz. They are both set to be 0.18 V_{pp} from 0.65 V to 0.83 V to reduce the RF noises on the electronic logic output signal, radiated from the bonding wires. EO switches thus operate in carrier-injection modes and the speed is limited.

from one horizontal waveguide is collected by the PD while light from the other waveguide is blocked by the on-off switch. In Figs. 5(e) and 5(f), there are two high levels for the output currents. Here the higher level corresponds to the case when both of the two waveguides pass light while the other level corresponds to the case when only one waveguide passes light. They are both judged as logic "1". In Figs. 5(c)-5(h), there are some positive spikes between two consecutive "0"s and some negative spikes between two consecutive "1"s, which have been well explained in the previous works [3], [5]. The spikes do not affect the correct decoding process since they only occur in the bit transition regions. Furthermore, in order to implement a cascadable logic circuit, the output electronic signals should be binary levels which can thus drive next circuits. Since there are two different logic "1" levels and one logic "0" level in the OR functions as shown in Figs. 5(e)-5(f), a current comparator with a chosen threshold current is needed to mold the outputs into binary levels [9].

Noted that, these reconfigurable logic operations with such a speed of 270 MHz could be applied in encryption for real-time secure multimedia delivery [10] as well as in autonomous driving based on light detection and ranging (Lidar) systems [11] where the speeds of input signals are not fast but low latencies in signal processing are highly desired. Furthermore, compared with logic operations in all electrical domain, directed-optical logic operations here have low latencies and are immune to electromagnetic interference by using the photonic circuit [12] while the exist RF radiation noises above can be effectively reduced by enlarging the distances between bonding wires [8].

V. Conclusion

We demonstrated a scalable and reconfigurable directed-optical circuit enabled by a single-wavelength light based on an array of integrated optical switches and PDs. By reconfiguring the small–scale circuit, arbitrary two-input combinational logic functions are realized in the the proof-of-concept demonstration. In this demonstration, the electronic logic input signals with low V_{pp} are chosen to decrease the RF radiation noise on the electronic output signal. Thus, the EO switches need to operate in carrier-injection modes which limit the speed of logic circuit to be 270 Mb/s. Since the MRR based EO switches can operate at a speed of multi-GHz at the carrier-depletion mode with a large reverse bias voltage [3], we expect a GHz operation is possible after minimizing the RF radiation noises from the large reverse bias voltages. A further increase in speed and a reduction in switching energy would be attained by using p-n depletion-type EO micro disk resonators [13] in Fig. 1 instead of the MRRs.

References

[1] J. Hardy and J. Shamir, "Optics inspired logic architecture," *Opt. Express*, vol. 15, no. 1, pp. 150–165, Jan. 2007.
[2] Q. F. Xu and R. Soref, "Reconfigurable optical directed-logic circuits using microresonator-based optical switches," *Opt. Express*, vol. 19, no. 6, pp. 5244–5259, Mar. 2011.
[3] C. Y. Qiu, W. L. Gao, R. Soref, J. T. Robinson, and Q. F. Xu, "Reconfigurable electro-optical directed-logic circuit using carrier-depletion micro-ring resonators," *Opt. Lett.*, vol. 39, no. 24, pp. 6767–6770, Dec. 2014.
[4] Y. H. Tian *et al.*, "Experimental demonstration of a reconfigurable electro-optic directed logic circuit using cascaded carrier-injection micro-ring resonators," *Sci. Rep.*, vol. 7, Jul. 2017, Art. no. 6410.
[5] L. Zhang *et al.*, "Demonstration of directed XOR/XNOR logic gates using two cascaded microring resonators," *Opt. Lett.*, vol. 35, no. 10, pp. 1620–1622, 2010.
[6] R. Dube-Demers, S. LaRochelle, and W. Shi, "Ultrafast pulse-amplitude modulation with a femtojoule silicon photonic modulator," *Optica*, vol. 3, no. 6, pp. 622–627, Jun. 2016.
[7] L. Vivien *et al.*, "Zero-bias 40 Gbit/s germanium waveguide photodetector on silicon," *Opt. Express*, vol. 20, no. 2, pp. 1096–1101, Jan. 2012.
[8] W. H. Chen *et al.*, "A 6-Gb/s wireless inter-chip data link using 43-GHz transceivers and bond-wire antennas," *IEEE J. Solid-State Circuits*, vol. 44, no. 10, pp. 2711–2721, Oct. 2009.
[9] D. A. Freitas and K. W. Current, "CMOS current comparator circuit," *Electron. Lett.*, vol. 19, no. 17, pp. 695–697, Aug. 1983.
[10] A. Pande and J. Zambreno, "A reconfigurable architecture for secure multimedia delivery," in *Proc. 23rd Int. Conf. VLSI Design*, Jan. 2010, pp. 258–263.
[11] Q. Li, L. Chen, M. Li, S.-L. Shaw, and A. Nuchter, "A sensor-fusion drivable-region and lane-detection system for autonomous vehicle navigation in challenging road scenarios," *IEEE Trans. Veh. Technol.*, vol. 63, no. 2, pp. 540–555, Feb. 2014.
[12] J. Capmany, B. Ortega, D. Pastor, and S. Sales, "Discrete-time optical Processing of microwave signals," *J. Lightw. Technol.*, vol. 23, no. 2, pp. 702–723, Feb. 2005.
[13] Z. F. Ying *et al.*, "Silicon microdisk-based full adders for optical computing," *Opt. Lett.*, vol. 43, no. 5, pp. 983–986, Mar. 2018.